# Reconstructing the Excitation Energy of $^{15}$N After an $^{16}$O$(p, 2p)$ Reaction with a Geant4 Simulation

Jeremiah Hugo, Department of Physics, College of the Holy Cross

University of Tokyo Research Internship Program, Yokoyama-Nakajima Research Group, Summer 2024

# 1 Introduction

## 1.1 Super-Kamiokande Dilemma

At the Super-Kamiokande (Super-K), the world's largest underground water Cherenkov detector, particle physicists are aiming to be the first to observe the Diffuse Supernova Neutrino Background (DSNB) by detecting inverse beta decay ($\bar{\nu}_e + p \rightarrow e^+ + n$). The DSNB is, theoretically, composed of many neutrinos that were birthed from core collapse supernova – massive stars that exploded during the last stage of their thermonuclear evolution. These neutrinos are racing towards the Earth, and the Super-K's trying to catch them. Part of this background consists of Neutral Current Quasi-Elastic (NCQE) interactions of atmospheric neutrinos with $^{16}$O. Together, the two reactions in Eqs. 1 and 2 imitate the signal of the DSNB, which, in reality, is produced by a positron and neutron pair.

$$\nu +^{16} O \rightarrow \nu +^{15} N^* + p \tag{1}$$

$$\nu +^{16} O \rightarrow \nu +^{15} O^* + n \tag{2}$$

Despite this knowledge, pinpointing such a pair from the DSNB signal with water Cherenkov detectors like the Super-K is challenging. The following phenomena hinder the efforts of particle physicists: (1) the de-excitation gammas from $^{15}$N$^*$ and $^{15}$O$^*$ imitate the $e^+$ signal; (2) the neutrons that are created when they are scattered off of $^{16}$O nuclei during primary and secondary interactions; and (3) the de-excitation gammas produced during secondary interactions, like the ones from $^{15}$N$^*$ and $^{15}$O$^*$, copy the $e^+$ signal. Consequently, the systematic uncertainty associated with the NCQE process is, at a minimum, 60%. Particle physicists at Super-K would like to decrease this uncertainty to at least 10%, and Professor Nakajima et al.'s SAMURAI proposal can potentially resolve the Super-K dilemma [4].

## 1.2 Neutrino Physics

Before diving into the theory of the SAMURAI proposal, the relevant neutrino physics transpiring in the Super-K must be reviewed. Neutrinos respond to gravity due to their trace amount of mass, but they primarily engage in weak interactions (Since they are electrically neutral, neutrinos are immune to the strong and electromagnetic forces). There are two types of weak interactions: charged current (CC) and neutral current (NC). A different boson is assigned to each current: the W boson for CC interactions and the Z boson for NC interactions. When the interactions are quasi-elastic, the neutrino collides with a nucleon that is bound to a nucleus, and is scattered off at an angle. This collision would be completely elastic if none of the participants in the collision were attached to anything else following the collision.

# 2 Experimental Method

## 2.1 Experimental Apparatus

Fig. 1 displays the experimental setup of the SAMURAI proposal. In the center lies the STRASSE liquid hydrogen (LH2) target, which has a length of 150 mm and a diameter of 31 mm. Surrounding the STRASSE target are three types of detectors: (1) the STRASSE tracker, which envelops the target and consists of two layers of silicon detectors; (2) the neutron detectors, which detect the neutrons that are knocked out during the interactions inside the target; and (3) the CATANA detector, which is composed of 140 CsI crystals doped with Na that are 23° to 90° relative to the beam axis and measures the energies of the protons and gammas with calorimetry. Henceforth, the scope of this report will be limited to the STRASSE target [4].

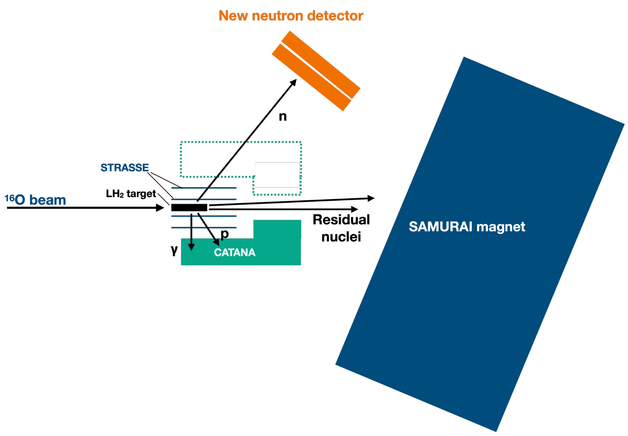


Figure 1: The experimental apparatus.

## 2.2 Inverse Kinematics Method

To study the interactions between neutrinos and $^{16}$O nuclei, particularly NCQE interactions, the inverse kinematics method must be employed. In inverse kinematics, an ion beam is fired at a light nuclear target like hydrogen or deuterium. From this interaction, several pieces of information can be extracted: (1) nucleons that recoiled; (2) fragments that are boosted forward in that they exit the container of the target; and (3) gammas that result from the de-excitation of ions. With the inverse kinematics method, all the residual nuclei and decay products, as a function of the excitation energy of $^{15}$O and $^{15}$N, can be measured. Consequently, observables related to the neutrino interactions with $^{16}$O can be accurately predicted.

## 2.3 Target Reaction: $^{16}$O (p, 2p)

When an $^{16}$O beam is fired at the LH2 target, it travels through the LH2 medium and triggers many events. Since these events do not occur within a vacuum, the beam loses energy and momentum before it reacts with the protons. The $^{16}$O (p, 2p) reaction, in particular, is the event of interest. As shown in Fig. 2, two protons, along with a $^{15}$N nucleus, are produced. This $^{15}$N nucleus can be excited and, theoretically, has a maximum excitation energy of 50 MeV.

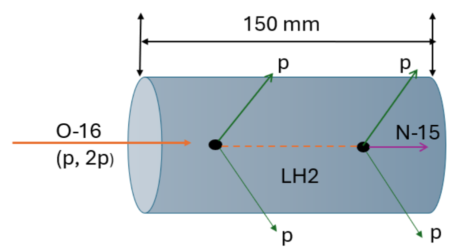


Figure 2: The event of interest in the target.

# 3 Data Analysis Method

## 3.1 Firing Protons & Muons At Several Material Media

Prior to simulating the SAMURAI proposal, it is beneficial to elucidate the relationship between several types of material media that particles can pass through and the energy that these particles deposit in these material media. To begin data analysis, a box with dimensions of 3 cm × 3 cm × 1 mm was constructed in Geant4, a simulation toolkit [2]. 600 MeV of protons and muons were fired at this box, which was created with the following elements: LH2, C, Al, Fe, Sn, and Pb. It was observed that, when protons were fired, the mean beam energy depositions that Geant4 calculated had increased as the element material changed from LH2 to Pb. To calculate the mean energy deposition rates of the protons, Eq. 3

was applied. It was observed that, as the element material changed from LH2 to Pb, the protons' mean energy rates decreased. The same trends were observed when muons were fired at the box (Muons, however, will be irrelevant for the rest of this report). All of the aforementioned values can be found below in Tables 1 and 2.

To compare the theoretical and experimental mean energy loss rates, the momenta of a proton and a muon were calculated using Eq. 4. The proton has a momentum of 1.219 GeV/c while the muon has that of 0.698 GeV/c. Next, the percent errors for all of the mean energy rates were calculated by finding the absolute difference between the experimental mean energy rates in Fig. 3 and the theoretical mean energy rates and dividing this difference by the experimental mean energy rates. Unfortunately, the percent errors did not always indicate that the theoretical and mean energy loss rates were consistent with each other.

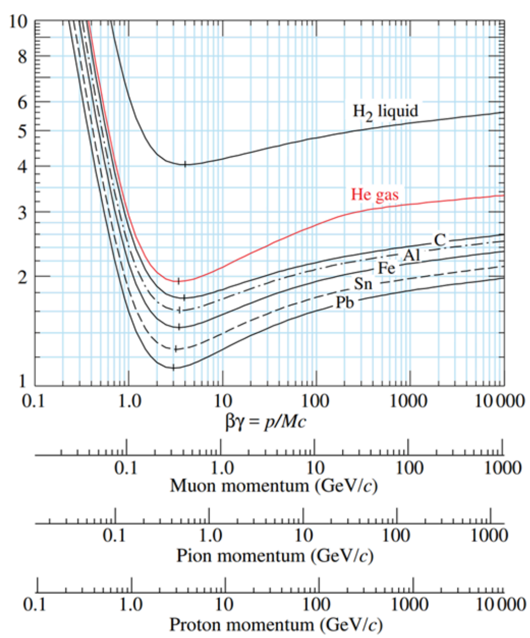


Figure 3: Each curve corresponds to a different element. Only He was disregarded. The experimental mean energy rates that were compared to their theoretical counterparts were approximated as the lowest y-values of each curve.

$$\left\langle -\frac{dE}{dx} \right\rangle = \frac{\text{Mean Beam Energy Deposition}}{\text{Target's Length} \cdot \text{Target's Material Density}} \tag{3}$$

$$p = \frac{\sqrt{T^2 + 2mTc^2}}{c} \tag{4}$$

## 3.2 Missing Mass Method

One observable that can be predicted is the excitation energy of $^{15}$N following an $^{16}$O (p, 2p) reaction. This energy can be determined using the missing mass method (Eq. 5) [3].

$$E_x = \sqrt{(E_{\text{beam}} + E_{\text{tgt}} - E_1 - E_2)^2 - \left(\vec{P}_{\text{beam}} - \vec{P}_1 - \vec{P}_2\right)^2} - M_{\text{frag}} \tag{5}$$

The following are the variables in Eq. 5:

- $E_{beam}$: the total energy of the $^{16}$O beam at the moment the beam hits a proton;
- $E_{tgt}$: the rest-mass energy of the LH2 target;
- $E_1$ and $E_2$: the total energies of protons 1 and 2, respectively, which can both be found with Eq. 6;
- $P_{beam}$: the total momentum of the $^{16}$O beam at the moment the beam hits a proton, which can be found with Eq. 7;
- $P_1$ and $P_2$: the Lorentz momenta of protons 1 and 2, respectively; and
- $M_{frag}$: the mass of the fragment, namely, the $^{15}$N nucleus.

$$E = \sqrt{(pc)^2 + (mc^2)^2} \tag{6}$$

$$p = \frac{\sqrt{E^2 - (mc^2)^2}}{c} \tag{7}$$

Although the above is known, one cannot proceed yet. First, one must identify the locations of each $^{16}$O (p, 2p) reaction inside the LH2 target to find $E_{beam}$

Table 1: Mean Energy Rates for Protons

| Protons | LH2 | C | Al | Fe | Sn | Pb |
|---|---|---|---|---|---|---|
| **Geant4 Mean (MeV)** | 0.0333326 | 0.524522 | 0.580367 | 1.51963 | 1.13241 | 1.75454 |
| **Mean Energy Rate (MeV · cm² / g)** | 4.70799 | 2.62261 | 2.150304 | 1.929934 | 1.549124 | 1.101321 |
| **Percent Error** | 9.49 | 38.03 | 26.49 | 24.51 | 19.16 | 37.67 |

Table 2: Mean Energy Rates for Muons

| Muons | LH2 | C | Al | Fe | Sn | Pb |
|---|---|---|---|---|---|---|
| **Geant4 Mean (MeV)** | 0.0238449 | 0.31531 | 0.396935 | 1.07757 | 0.860171 | 1.24999 |
| **Mean Energy Rate (MeV · cm² / g)** | 3.367924 | 1.57655 | 1.47067 | 1.36598 | 1.176705 | 1.10132 |
| **Percent Error** | 25.33 | 9.91 | 10.87 | 8.93 | 9.48 | 37.67 |

and $P_{beam}$. In other words, the relationship between the $^{16}$O beam's energy deposition and the length of the LH2 target must be investigated.

### 3.3 Proton & $^{16}$O Beam Energy Deposition

In Geant4, a cylinder with a radius of 25 mm and varying lengths was created. The initial length was 5 mm, and it was increased by 10 mm increments until 150 mm was reached (The final length will most likely be the target's thickness during a real implementation of the SAMURAI proposal). The particle gun fired 1,000 protons with an energy of 200 MeV/nucleon. In Fig. 4, the proton beam's energy loss and the target's thickness are on the vertical and horizontal axes, respectively.

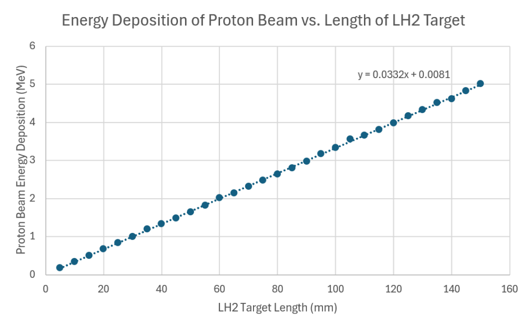


Figure 4: 1,000 protons were fired with an energy of 200 MeV/nucleon.

Once again, a cylinder with the same geometry was constructed. As for the particle gun, it fired 1,000 $^{16}$O nuclei with an energy of 200 MeV/nucleon. In Fig. 5, the $^{16}$O beam's energy loss and the target's thickness are on the vertical and horizontal axes, respectively.

Clearly, there is a linear relationship between the beam's energy loss and the target's length, regardless of the particles that are fired. In addition, the graphs have slopes of approximately 0.03 MeV/mm and 2.17 MeV/mm, respectively.

In Section 3.1, the theoretical mean energy rates had been calculated merely through dimensional analysis (it is known that the unit is MeV · cm$^2$ / g), but they can be calculated more formally with Bethe's Equation (Eq. 8). This equation allows one to find the expectation value of the energy loss rate of a moderately relativistic charged heavy particle.

$$\left\langle -\frac{dE}{dx} \right\rangle = Kz^2 \frac{Z}{A} \frac{1}{\beta^2} \left( \frac{1}{2} \ln \frac{2m_e c^2 \beta^2 \gamma^2 W_{\max}}{I^2} - \beta^2 - \frac{\delta(\beta\gamma)}{2} \right) \tag{8}$$

For protons and $^{16}$O nuclei, the following are rele-

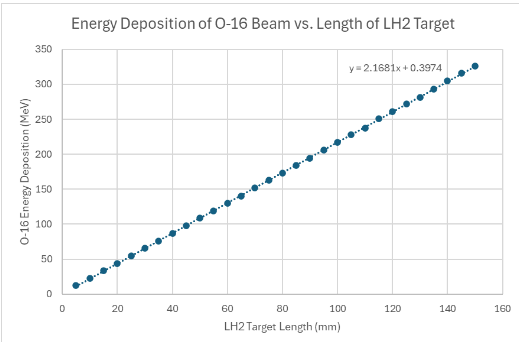


Figure 5: 1,000 $^{16}$O nuclei were fired with an energy of 200 MeV/nucleon.

vant to applying the equation:

- $K$: the coefficient of -dE/dx (0.307075 MeV $\cdot$ cm$^2$ / mol)
- $z$: the charge number of the incident particle (+1 for a proton; +8 for an $^{16}$O nucleus)
- $Z$: the atomic number of the absorber (1 for LH2)
- $A$: the atomic mass of the absorber (1 g/mol for LH2)
- $\beta$: the relativistic factor (0.42, the ratio between the velocity of a proton, or an $^{16}$O nucleus, and the speed of light; this was calculated using Eqs. 9 and 10).

$$\gamma = \frac{mc^2 + T}{mc^2} \tag{9}$$

$$\beta = \sqrt{1 - \frac{1}{\gamma^2}} \tag{10}$$

The rest of the equation can be ignored for the sake of simplicity.

With Bethe's Equation, a 64:1 ratio between the theoretical mean energy losses of an $^{16}$O nucleus and a proton is derived. This ratio is determined by the charge ratio of the particles in question. More specifically, an $^{16}$O nucleus has a charge of +8 while a proton has a charge of +1, so when these particles' charges are squared and their ratio is calculated, the result is 64:1.

### 3.4 Reconstruction Method for $^{16}$O Beam

In Geant4, the experimental setup of the SAMURAI proposal can be visualized on an xz-plane as shown in Fig. 6. Seeing that the target's front and back ends lie at -4775 mm and -4625 mm on the z-axis, respectively, 4775 must be added to the z-coordinate at which the beam meets a proton inside the target. When this sum is multiplied by the slope of the graph in Fig. 5, the energy deposition correction factor (CF) is as follows:

$$E_{\text{loss correction factor}} = 2.17(z + 4775). \tag{11}$$

Now, this correction factor can be incorporated into the missing mass method.

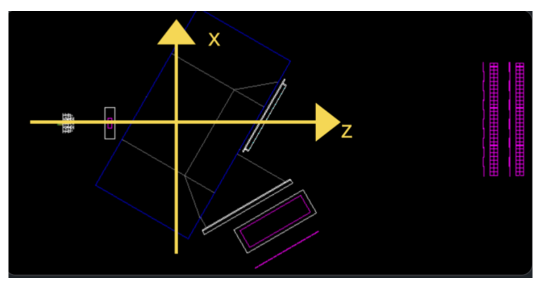


Figure 6: The experimental setup in the Geant4 simulation. The LH2 target is the white rectangle containing the pink rectangle and is bisected by the z-axis.

The missing mass method, as it is used in Geant4, is illustrated with the following steps:

1. Create counters for the $^{15}$N nuclei and the protons. Each counter will increment by one if Geant4 examines the secondary particles – particles created through secondary interactions – and finds that their respective Particle Data Group Codes (PDGCodes) match that of $^{15}$N nuclei and protons.

2. Ignore all events in which the $^{15}$N nuclei counter is not one or the proton counter is not two.

3. Initialize and declare the three-dimensional vectors for the Lorentz momenta of the protons, which are found after several steps. Every time one $^{15}$N nucleus and two protons are counted, the $^{16}$O (p, 2p) counter increments by one. As a result, Geant4 iterates through the initial momenta of the secondary particles, and when two secondary particles' PDGCodes match that of a proton, the momenta of these protons are assigned.

4. Create a three-dimensional vector for the z-coordinate of the $^{16}$O beam prior to the event of interest. Compute this z-coordinate by passing the Secondary Data array to the GetMCTruthVertex function.

5. Combine the kinetic energy of the beam immediately before the $^{16}$O (p, 2p) reaction with the rest mass energy of the beam.

6. Subtract the energy loss correction factor from the sum in Step 5; the result is the total energy of the beam the moment before the reaction.

7. Substitute the total energy of the beam and the rest-mass energy of the beam into Eq. 7, with c = 1.0, to calculate the total momentum of the beam.

8. Set the rest-mass energy of the proton equal to the energy of the target.

9. Substitute the momentum of proton 1 and the rest-mass energy of a proton into Eq. 6 and calculate the energy of proton 1. The same applies to proton 2.

10. Substitute all of the above variables into Eq. 5 to calculate the excitation energy of the current loop.

11. Add this excitation energy to the variable that holds the sum of the excitation energies in each loop.

12. When the for loop is finished, the sum of the excitation energies is divided by the $^{16}$O (p, 2p) counter to yield the mean excitation energy of $^{15}$N.

# 4 Results & Analysis

Over 183 events, a mean excitation energy of 7.391 MeV is calculated for $^{15}$N [1].

With ROOT, a data analysis software, histograms of the excitation energy distributions can be generated.

Fig. 7 illustrates the excitation energy distribution over the length of the target, while Table 3 summarizes the data as the total number of events, the mean excitation energy, and the standard deviation and standard error of the excitation energy.

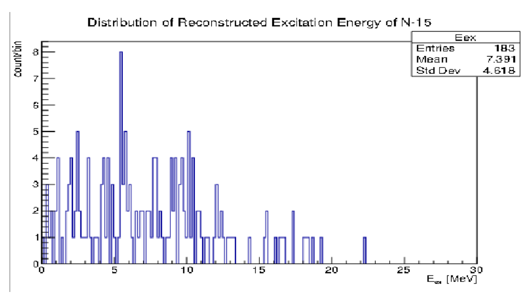


Figure 7: Distribution of Reconstructed Excitation Energy of $^{15}$N Over Whole Target (MeV)

Figs. 8-11 display the distributions of the excitation energies for the front and back halves of the LH2 target when the energy loss correction factor is included and when it is not. The front half is from the end of the target closest to the particle gun (0

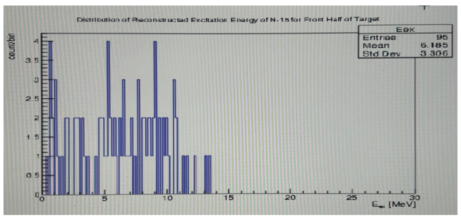


Figure 8: The beam's energy loss is considered for the front half of the target.

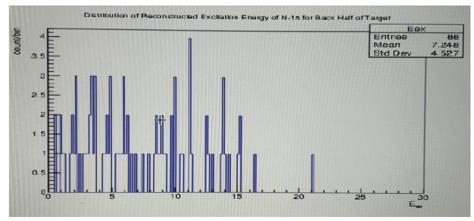


Figure 9: The beam's energy loss is considered for the back half of the target.

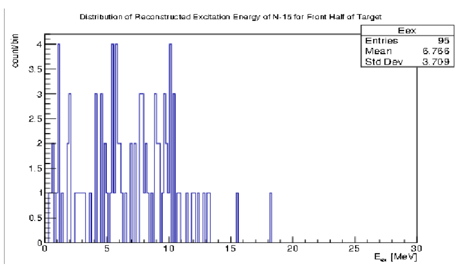


Figure 10: The beam's energy deposition is ignored for the front half of the target.

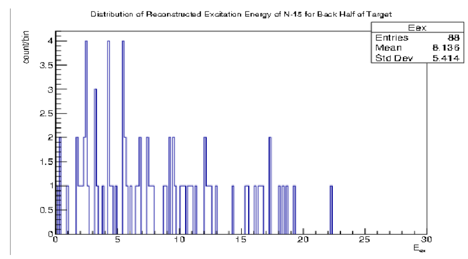


Figure 11: The beam's energy deposition is ignored for the back half of the target.

Table 3: Reconstructed Excitation Energy of $^{15}$N Over Whole Target (MeV)

| | |
|---|---|
| **Events** | 183 |
| **Mean** | 7.391 |
| **Standard Deviation** | 4.618 |
| **Standard Error** | 0.341 |

mm) to the midpoint of the target (75 mm), while the back half is from the midpoint to the other end of the target (150 mm). Table 4 not only includes the same types of data as Table 3 for the front and back halves of the target, but also presents the difference in the means of these halves, the uncertainties associated with these differences, and the significance ratios.

Before creating the Geant4 simulation, it was expected that the mean excitation energy of $^{15}$N should not depend on the location of the events inside the LH2 target. To assess whether there is a significant difference between the front and back halves, both with and without the correction factor, the differences in means is divided by the uncertainties to yield the significance ratios. Since these ratios are less than 2, the observed differences between the front and back halves, whether or not there is a correction factor, are likely statistically insignificant. Additionally, when the correction factor is implemented, the mean excitation energy decreases by 0.581 MeV and 0.888 MeV for the front and back halves, respectively. These decreases indicate that the correction factor is functioning as intended.

Table 4: Reconstructed Excitation Energy of $^{15}$N for Front & Back Halves (MeV)

| | **Front Half, CF** | **Back Half, CF** | **Front Half, no CF** | **Back Half, no CF** |
|---|---|---|---|---|
| **Events** | 95 | 88 | 95 | 88 |
| **Mean** | 6.185 | 7.248 | 6.766 | 8.136 |
| **Standard Deviation** | 3.306 | 4.527 | 3.709 | 5.414 |
| **Standard Error** | 0.339 | 0.483 | 0.381 | 0.577 |
| **Difference in Means** | -1.063 | | -1.370 | |
| **Uncertainty** | 0.590 | | 0.691 | |
| **Significance Ratio** | 1.802 | | 1.983 | |

# 5 Discussion

Using a Geant4 simulation, the reconstruction method for an $^{16}$O beam was created. This method aims to accurately reconstruct the excitation energy of $^{15}$N following an $^{16}$O (p, 2p) reaction with the missing mass method in mind. It also yields distributions of the reconstruction excitation energy that are independent of the position of the $^{16}$O (p, 2p) reactions. However, this interpretation is dubious, given that the total number of events is as low as 88.

It is also important to note that the reconstruction method for an $^{16}$O beam provides two sets of data: (1) the mean excitation energy of $^{15}$N; and (2) the true excitation energy for each event. While the mean excitation energy of $^{15}$N can be determined through Geant4 simulations, the true excitation energy for each event can be extracted from the Root histograms. In the future, it would be favorable to test the accuracy with which the reconstruction method calculates the excitation energy. This test entails a comparison between the reconstructed excitation energy of $^{15}$N and the true excitation energy for each event.

To further improve this method, one should not calculate the energies of the protons. Instead, he or she could measure these quantities with the CATANA and STRASSE detectors.

# 6 Acknowledgements

UTRIP was more than an internship; it was an experience that combined my interests in physics and Japanese culture in one package. I am grateful to Prof. Nakajima and Prof. Yokoyama for welcoming me into their lab and allowing me to delve into particle physics further. Special thanks to Mizuno-san, who generously gave much of his time to assist me throughout my stay in Japan. Prof. Nakajima's guidance, paired with Mizuno-san's, brought the reconstruction method to fruition. It was also a pleasure to meet fellow physics majors like Bilguun and Ching Yu. As for the Japanese side of the internship, I extend my thanks to the folks at the UTRIP Office and FUTI who made this trip possible.

# References

[1] R. Brun and F. Rademakers. *ROOT: An Object-Oriented Data Analysis Framework*, 1997. Accessed: 2024-08-19.

[2] Geant4 Collaboration. *Book for Application Developers*, release 11.2 edition, 2023. Available at: `http://geant4-userdoc.web.cern.ch/geant4-userdoc/UsersGuides/ForApplicationDeveloper/BackupVersions`.

[3] H.N. Liu et al. "STRASSE: a silicon tracker for quasi-free scattering measurements at the ribf". *The European Physical Journal A*, 59, 2023.

[4] Y. Nakajima et al. "SAMURAI proposal: Study of $^{16}$O(p, 2p) and $^{16}$O(p, pn) reactions for precise neutrino observation at giant water cherenkov detectors". 2023.